ELSEVIER

Physica D 102 (1997) 285–299

PHYSICA D

Initiation of propagation in a one-dimensional excitable medium [1]

John C. Neu [a], R. Stephen Preissig, Jr. [b], Wanda Krassowska [b,c,*]

[a] *Department of Mathematics, University of California at Berkeley, CA, USA*

[b] *Department of Biomedical Engineering, Duke University, Durham, NC 27708-0281, USA*

[c] *Duke-North Carolina NSF/ERC, Duke University, USA*

Received 8 December 1995; revised 26 July 1996; accepted 23 August 1996

Communicated by C.K.R.T. Jones

Abstract

This study examines the initiation of propagation in a one-dimensional fiber by local stimulation with a small electrode. The membrane dynamics is based on the generic FitzHugh–Nagumo model, reduced in a singular limit to a nonlinear heat equation. A steady-state solution of this nonlinear heat equation defines the critical nucleus, a time-independent distribution of potential that acts as a threshold for propagating wavefronts. The criterion for initiation of propagation from the initial conditions on potential is obtained by re-writing the nonlinear heat equation as a gradient flow of an energy and projecting this gradient flow onto an approximate solution space. Assuming that the evolving potential has a shape of a Gaussian pulse, the solution space consists of the amplitude of the pulse, a, and the inverse of its width, k. The evolution of the potential is visualized on the (a, k) phase plane in which the rest state is a stable node and the critical nucleus solution is a saddle point. The criterion for initiating propagation takes the form of a pair of separatrices that bisect all possible pulse widths. For a specific pulse width, the separatrices determine the minimum amplitude necessary to start propagation. Infinitely broad pulses (space-clamped fiber) require amplitude equal to the membrane excitation threshold. As the width of the pulse decreases, the requirement on the amplitude grows. In a limit of very narrow pulses, the pulse width and the amplitude are related by a linear relationship corresponding to a constant charge delivered by the pulse.

PACS: 87.22.Jb; 41.20.Bt; 02.60.Lj

Keywords: Reaction–diffusion equation; FitzHugh–Nagumo model; Propagation; Electric stimulation; Transmembrane potential; Luminal length

1. Introduction

Consider an infinite one-dimensional fiber with membrane dynamics described by the generic FitzHugh–Nagumo (FN) model [1,2]. The state variables, transmembrane potential v and inactivation variable y are governed by the following equations:

$$v_t = v_{xx} - f'(v) - y, \qquad y_t = \varepsilon(\alpha v - y). \tag{1}$$

In (1), ε is a small parameter, α is a constant, and $f'(v)$ is a cubic polynomial shown in Fig. 1(a),

$$f'(v) = v(\mu - v)(1 - v). \tag{2}$$

* Corresponding author. Tel.: (919) 660-5105; fax: (919) 660-5405; e-mail: wanda@eel-mail.mc.duke.edu.

[1] Supported in part by the National Institutes of Health grant HL54071-01, the National Science Foundation grant BES-9409026, the National Science Foundation Engineering Research Center grant CDR-8622201, and the Thomas Lord Foundation of North Carolina

PII S0167-2789(96)00203-5

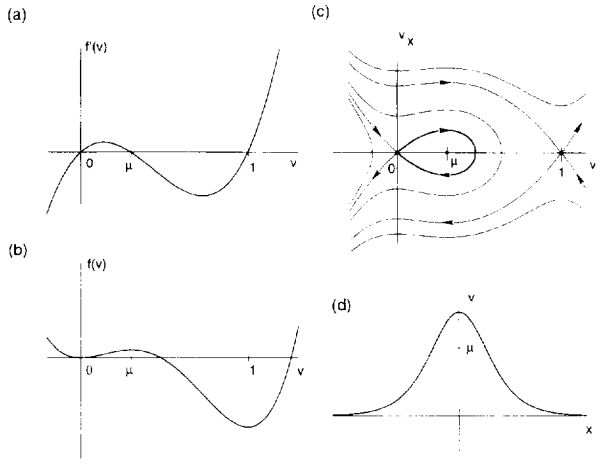

Fig. 1. (a) The cubic current–voltage relationship $f'(v)$ which in the NLHE (4) represents the excitability of the membrane. Rest state is at $v = 0$, threshold at $v = \mu$, and the excited state at $v = 1$. (b) The antiderivative $f(v)$ of this current–voltage relationship. (c) The (v, v_x) phase plane of the NLHE (4). Arrows indicate the direction of increasing x. The homoclinic orbit shown in a heavy solid line corresponds to the critical nucleus solution shown in Panel (d).

The roots of the cubic, $v = 0$, μ, and 1, correspond to the rest state, threshold, and excited state of the membrane. In order for (1) to give rise to a propagating wavefront, μ must satisfy $0 < \mu < \frac{1}{2}$.

If a brief external electric stimulus is applied to a fiber at the rest state through a small electrode, it instantaneously charges the membrane and causes a local change in the transmembrane potential. This type of external stimulation can be represented by initial conditions at time $t = 0$:

$$v(x, 0) = v_0(x) \quad \text{and} \quad y(x, 0) = 0. \tag{3}$$

The initial distribution of the transmembrane potential, $v_0(x)$, is spatially localized, with $v_0(x) \to 0$ as $|x| \to \infty$. The total charge and energy associated with the initial condition (3) are integrals proportional to $\int_{-\infty}^{\infty} v_0(x)\,dx$ and $\int_{-\infty}^{\infty} v_0^2(x)\,dx$, respectively. Both are assumed to be finite.

Under certain conditions, initial distribution $v_0(x)$ elicits an action potential which gives rise to a propagating wavefront. Propagating wavefronts have been studied in great detail [3–7].

In comparison, the process by which an initial distribution caused by the stimulus develops into a full-fledged propagating wavefront has received much less attention. In 1937, Rushton introduced a concept of the liminal length. According to this hypothesis, there is a minimum length of a fiber that $v_0(x)$ must raise above the excitation threshold in order to initiate the propagating wavefront [8]. This concept has been followed in more recent studies and appears to be consistent with experimental data [9,10]. However, the analysis leading to the liminal length hypothesis was based either on a linear model of the excitable membrane [9] or on a steady-state solution to the nonlinear model [11]. By necessity, such models give an incomplete picture of the initiation of the propagating wavefront.

A mathematically precise characterization of the initiation of propagation has been carried out in a singular limit of Eq. (1), $\varepsilon \to 0$. Thus, the inactivation variable is kept at its rest state, $y = 0$, and the transmembrane potential satisfies the nonlinear heat equation (NLHE),

$$v_t = v_{xx} - f'(v). \tag{4}$$

McKean and Moll [12], using a piecewise linear representation of $f'(v)$, demonstrated that for the initial data $v_0(x)$ corresponding to the local stimulation with a single electrode, there exists a threshold surface in the space of initial data that separates subcritical $v_0(x)$, which decay to zero, from the supercritical $v_0(x)$, which expand into a pair of propagating wavefronts. This threshold was shown to form a smooth surface of codimension 1 in the space of initial data. Aronson and Weinberger [13] used a maximum principle to investigate sufficient conditions for sub- and super-critical initial data.

The actual construction of the threshold surface was undertaken numerically by Moll and Rosencrans [14] and Moll [15]. The method is based on the result of McKean and Moll [12] which states that if $v_0(x)$ is on the threshold surface, then $v(x, t)$ would remain on this surface and in the limit $t \to \infty$, $v(x, t)$ would converge to a solution of the time-independent equation. This allowed Moll and Rosencrans to trace the threshold surface by numerically solving NLHE (4) with the initial data $v_0(x)$ lying on this surface. This study

chose as $v_0(x)$ a rectangular pulse. Consequently, the threshold surface was expressed as a relation between the amplitude and the width of the initial pulse.

Our study takes a different approach to examining the evolution of the initial pulse and determining the criterion for the initiation of propagation. The basic idea is to use the amplitude a and the width $1/k$ of the pulse to characterize not only the initial data $v_0(x)$, as in the work of Moll and Rosencrans [14], but also the evolving pulse $v(x,t)$. Specifically, the full dynamics of the NLHE (4) is projected onto a two-dimensional space of Gaussian pulses,

$$v(x,t) = a(t)e^{-(k(t)x)^2}, \tag{5}$$

yielding a pair of ordinary differential equations (ODEs) that describe the evolution of $a(t)$ and $k(t)$. This simple projected dynamics produces a robust and almost a quantitative approximation not only to the threshold surface but also to the true dynamics of the NLHE (4).

The threshold phenomenon in the full FN system was studied by Terman [16], who demonstrated that the initial data (3) is superthreshold if ε is sufficiently small and $v_0(x)$ exceeds threshold μ over a sufficiently long interval of x. Our study complements this rigorous but abstract result with a concrete phenomenology. Combined asymptotics and numerical simulation allows us to observe that if $v_0(x)$ is sufficiently far from the threshold curve of the NLHE, then the effect of the inactivation variable y is a small perturbation, and to investigate new phenomena arising when $v_0(x)$ is very near the threshold curve.

This paper consists of four sections. Section 2 examines the steady-state solutions of the NLHE (4) and introduces a concept of the critical nucleus, a time-independent distribution $v_{cr}(x)$ that acts as a threshold for propagating wavefronts. Section 3 introduces the projected dynamics and uses it to formulate the criteria for the initiation of propagation. Section 4 compares the results obtained using the projected dynamics with the numerical solutions to the NLHE (4) and with the earlier results of Aronson and Wienberger [13], Moll and Rosencrans [14], and Moll [15]. Section 5 reintroduces the inactivation variable y and examines its role in the initiation of propagation. Finally, Section 6 summarizes the limitations of this study and relates the results to the liminal length hypothesis.

2. Critical nucleus

Consider the NLHE (4) with an initial condition $v(x,0) = v_0(x)$ such that $v_0(x) \to 0$ as $|x| \to \pm\infty$ and $v_0(x) > \mu$ in some interval. As $t \to \infty$, $v(x,t)$ either decays to zero or develops an expanding interval where v is nearly 1. The latter case is the propagation. A sufficient condition for either scenario can be found based on the time-independent solution of the NLHE [11,12]. This so-called critical nucleus solution satisfies an ODE,

$$v_{xx} - f'(v) = 0. \tag{6}$$

The first integral is

$$I = \tfrac{1}{2}v_x^2 - f(v), \tag{7}$$

where I is a constant of integration and $f(v)$ is

$$f(v) = \tfrac{1}{4}v^4 - \tfrac{1}{3}(1+\mu)v^3 + \tfrac{1}{2}\mu v^2. \tag{8}$$

Recall from (2) that $f'(v) = 0$ at $v = 0$, μ, and 1. Roots $v = 0$ and 1 are the minima of $f(v)$ and μ is a local maximum (Fig. 1(b)). Fig. 1(c) shows the (v, v_x) phase plane which consists of level curves oriented in the direction of increasing x. The trajectory that satisfies the condition $v_0(x) \to 0$ as $|x| \to \infty$ must have $I = 0$ and takes the form of a homoclinic orbit which starts from and returns to the rest point $(0,0)$. It corresponds to the critical nucleus solution $v_{cr}(x)$ depicted in Fig. 1(d).

If the distribution of the transmembrane potential in a fiber is equal to $v_{cr}(x)$, then the negative transmembrane current that flows in the proximity of the electrode and that depolarizes the membrane towards threshold is balanced by the positive, hyperpolarizing current away from the electrode. Hence, the critical nucleus solution represents a threshold for propagation. The solutions $v(x,t)$ smaller than $v_{cr}(x)$ decay to zero as $t \to \infty$, and the solutions larger than $v_{cr}(x)$ develop an expanding interval with v near 1. The rigorous proof that the solution to the NLHE (4) with the

initial conditions bounded above (below) by the critical nucleus solution always remains bounded below (above) the critical nucleus solution is based on the maximum principle [13].

Analytical expressions for the critical nucleus solution were computed by Noble [11] and McKean and Moll [12] for the piecewise linear approximations of $f'(v)$. Here, $v_{cr}(x)$ is computed for the cubic $f'(v)$ in an asymptotic limit $0 < \mu \ll 1$. In this limit, the amplitude of the critical nucleus is small, i.e., $|v_{cr}| \ll 1$. Accordingly, the cubic polynomial (2) can be approximated by a quadratic function,

$$f'(v) \sim v(\mu - v). \tag{9}$$

Hence, for the critical nucleus solution, integral (7) is approximated by

$$\tfrac{1}{2}v_x^2 - \tfrac{1}{2}\mu v^2 + \tfrac{1}{3}v^3 = 0. \tag{10}$$

The solution of this equation gives an expression for the approximate critical nucleus

$$v_{cr}(x) \sim \tfrac{3}{2}\mu \operatorname{sech}^2(\tfrac{1}{2}\sqrt{\mu}\, x). \tag{11}$$

The amplitude a and the width $1/k$ of this critical nucleus are

$$a = \frac{3}{2}\mu, \qquad \frac{1}{k} = \frac{2}{\sqrt{\mu}}. \tag{12}$$

Note that $a/k^2 = 6$, which is a constant independent of μ.

The critical nucleus acts as a propagation threshold for a one-dimensional fiber in the similar way μ acts as an excitation threshold for the space-clamped membrane. In the space-clamped case, if at any time t, $v(t) > \mu$, the transmembrane potential will grow towards the excited state, $v = 1$. Similarly, in a one-dimensional fiber case, if at any time t, $v(x,t) > v_{cr}(x)$, the potential in the whole fiber will grow towards the excited state by means of a propagating wavefront. However, in contrast to the space-clamped membrane, $v_0(x) > v_{cr}(x)$ is not a necessary condition for the initiation of propagation. Initial distribution $v_0(x)$ can be broader and of lower amplitude than v_{cr} and still result in propagation. Likewise, there exist $v_0(x)$ taller and narrower than v_{cr} that initiate propagation. Thus, the next section will develop a more general criterion for the initiation of propagation.

3. Initiation of propagation using projected dynamics

3.1. Energy of the NLHE and the projected gradient flow

For potentials $v(x,t)$ with $v(x,t) \to 0$ as $|x| \to \infty$, energy E can be defined as

$$E = \int_{-\infty}^{\infty} (\tfrac{1}{2}v_x^2 + f(v))\,\mathrm{d}x \tag{13}$$

and the NLHE (4) may be written as a gradient flow of the energy,

$$v_t = -\frac{\delta E}{\delta v}, \tag{14}$$

where $\delta E/\delta v$ is the variational derivative. The gradient flow structure of the NLHE has been used by Fife and McLeod [17] to characterize sub- and superthreshold initial conditions. These results, while rigorous, are qualitative in character. Here, the gradient flow of the NLHE is projected onto a two-dimensional approximate solution space formed by the amplitude and 1/width of a pulse. The resulting "projected dynamics" is a pair of the ODEs describing the temporal evolution of the amplitude and the width of the pulse. As will be demonstrated in Section 4, this projected dynamics, while nonrigorous, provides a good approximation to the dynamics of the NLHE (4).

The starting point is a parametric representation of the potential $v(x,t)$,

$$v(x,t) = V(\boldsymbol{a}(t), x), \quad \text{for all } t, \tag{15}$$

where $\boldsymbol{a}(t) = a_1(t), \ldots, a_N(t)$ is a time-dependent vector of parameters. The derivatives of V with respect to all a_i are linearly independent as functions of x, so none of the parameters $a_i(t)$ are redundant. Assuming that the exact solutions of the gradient system (14) are in the form (15), a system of ODEs for $\boldsymbol{a}(t)$ is readily derived.

Given a parametric representation of v (15), the time derivative v_t can be expressed as

$$v_t = \partial_j V \dot{a}_j. \tag{16}$$

Here, ∂_i denotes differentiation with respect to a_i, overdot denotes differentiation with respect to time, and there is a summation over the repeated index j. The gradient flow (14) implies

$$\partial_j V \dot{a}_j = -\frac{\delta E}{\delta v}, \tag{17}$$

where the functional derivative $\delta E/\delta v$ is evaluated with $v = V(\boldsymbol{a}, x)$. The form of (17) indicates that $\delta E/\delta v$ is a linear combination of $\partial_j V$, $j = 1, \ldots, N$. To extract the ODEs for $a_j(t)$, one must take the functional inner product of (17) with $\partial_i V$,

$$\left(\int_{-\infty}^{\infty} \partial_i V \partial_j V \, \mathrm{d}x \right) \dot{a}_j = -\int_{-\infty}^{\infty} \frac{\delta E}{\delta v} \partial_i V \, \mathrm{d}x. \tag{18}$$

The right-hand side has a clear significance: Setting $v = V(\boldsymbol{a}, x)$ in the total energy (13), E can be treated as a function of $\boldsymbol{a}$, $E = E(\boldsymbol{a})$. It follows from the definition of functional derivative that

$$\partial_i E = \int_{-\infty}^{\infty} \frac{\delta E}{\delta v} \partial_i V \, \mathrm{d}x \tag{19}$$

and (18) becomes

$$\left(\int_{-\infty}^{\infty} \partial_i V \partial_j V \, \mathrm{d}x \right) \dot{a}_j = -\partial_i E. \tag{20}$$

In linear algebraic notation, (20) is

$$M\dot{\boldsymbol{a}} = -\nabla E, \tag{21}$$

where the gradient operator is taken with respect to $\boldsymbol{a}$ and M is the $N \times N$ symmetric matrix with components

$$m_{ij} = \int_{-\infty}^{\infty} \partial_i V \partial_j V \, \mathrm{d}x. \tag{22}$$

Eq. (21) is the required system of ODEs that represents the dynamics of the gradient system (14).

3.2. Projected dynamics for the initiation of propagation

In the application to a localized stimulation of a one-dimensional fiber, an exact parametric representation of the solution is not known. Hence, the form of V in (15) must be an approximation. Consequently, the ODEs for the parameters will represent a projection of the gradient flow (14) onto the approximate solution space. In this study, the transmembrane potential v is assumed to have a shape of a Gaussian pulse given in (5). The rationale for choosing this particular form is that for narrow pulses, (5) is an asymptotic solution of the NLHE (4) (see Section 3.3). Of course, other choices, such as $a\,\mathrm{sech}^2(kx)$ that describes the critical nucleus solution, could be similarly justified, but (5) allows to determine the ODEs of (21) with a relative ease.

The determination of the ODEs for the projected dynamics will be carried out in the same asymptotic limit $0 < \mu \ll 1$ as the computation of the critical nucleus presented in the previous section. When the cubic polynomial (2) is approximated by quadratic (9), the NLHE (4) takes the reduced form

$$v_t = v_{xx} - v(\mu - v). \tag{23}$$

The threshold parameter can be removed from (23) by adopting these units of the variables:

$$\begin{array}{lccc} \text{variable} & v & x & t \\ \text{unit} & \mu & \dfrac{1}{\sqrt{\mu}} & \dfrac{1}{\mu} \end{array} \tag{24}$$

Making replacements $v \to \mu v$, $x \to x/\sqrt{\mu}$, and $t \to t/\mu$, the reduced NLHE (23) becomes

$$v_t = v_{xx} - v(1 - v). \tag{25}$$

The explicit form of the projected dynamics (21) based upon the Gaussian representation of v (5) is

$$\begin{aligned} \dot{a} &= -a(2k^2 + 1 - pa), \\ \dot{k} &= -k(2k^2 - qa), \end{aligned} \tag{26}$$

where p and q are constants

$$p = \frac{7}{6}\sqrt{\frac{2}{3}} \approx 0.9526, \qquad q = \frac{1}{3}\sqrt{\frac{2}{3}} \approx 0.2722. \tag{27}$$

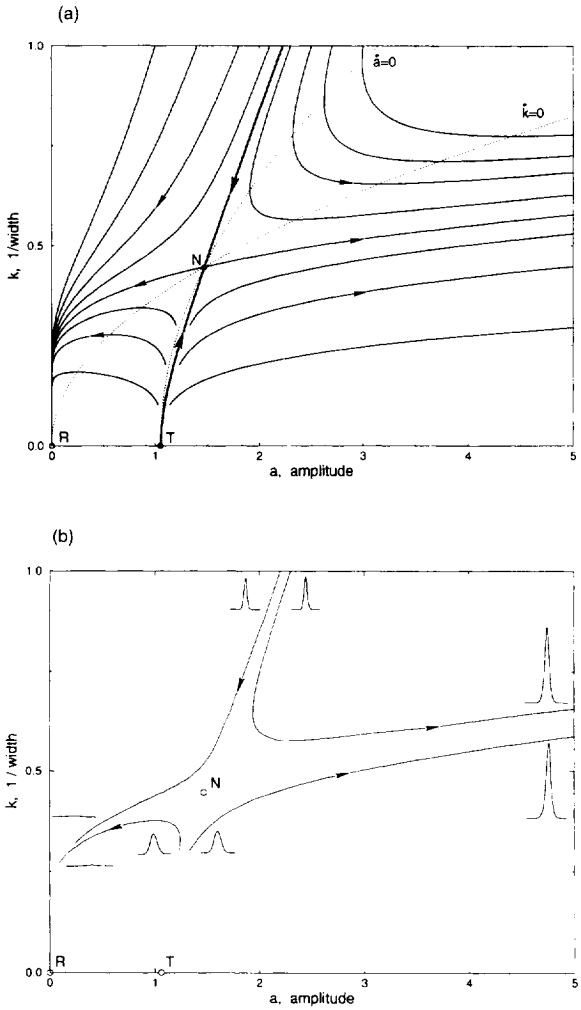

Fig. 2. (a) The phase plane (a, k) of the projected dynamics (26). The trajectories are drawn with solid lines, and the arrows indicate the direction of increasing time. The $\dot{a} = 0$ and $\dot{k} = 0$ nullclines are drawn with dotted lines. A stable node $R(0, 0)$ corresponds to the rest state, and a saddle point $N(1.47, 0.447)$ corresponds to the critical nucleus. The two stable manifolds of N drawn with a heavy solid line form separatrices that act as a threshold for propagation. Initial pulses to the left of the separatrices decay to zero, and initial pulses to the right give rise to propagating wavefronts. The unstable node $T(1.05, 0)$ is the threshold for infinitely broad pulses (space-clamp). It is slightly higher than the exact threshold $\mu = 1$ because of the Gaussian approximation of the pulse shape. (b) The evolution of the pulse along four representative trajectories of the (a, k) phase plane.

The phase plane of the projected dynamics (26) is depicted in Fig. 2(a). It has a stable node R at $(0, 0)$, which corresponds to the rest state, and a saddle point N at $(1.47, 0.447)$, which corresponds to the critical nucleus. The stable and unstable manifolds of the saddle point N divide the trajectories into four groups. Fig. 2(b) illustrates the evolution of the pulse along a representative trajectory in each group. The two stable manifolds of N, drawn with a heavy solid line in the (a, k) phase plane of Fig. 2(a), divide the phase plane into nonexcitable and excitable regions. Initial conditions to the left of these separatrices lead to $a \to 0$ as $t \to \infty$. These are the initial conditions that fail to start propagation. Initial conditions to the right lead to $a \to \infty$ in finite time. These are the initial conditions that succeed in starting propagation, even though the blowups themselves are not physical due to the truncated form of the NLHE (25). Hence, these two separatrices together define a relation between amplitude a and width $1/k$ corresponding to the threshold for propagation. The $k \to \infty$ limit of this curve is particularly significant, since it corresponds to initial stimulations whose length scales are much shorter than the length constant of the medium at rest. This case will be examined in the next section.

3.3. Asymptotic limits for $k \to \infty$

In the limit $k, a \gg 1$, the projected dynamics (26) achieves the reduced form

$$\dot{a} = -a(2k^2 - pa), \qquad \dot{k} = -k(2k^2 - qa). \tag{28}$$

Phase-plane trajectories of this reduced system are integral curves of the ODE

$$\frac{\mathrm{d}a}{\mathrm{d}k} = \frac{a}{k}\left(\frac{2k^2 - pa}{2k^2 - qa}\right). \tag{29}$$

This ODE is invariant under scalings of k and a which preserve a/k^2, so a new variable equal to a/k^2 can be defined. Eq. (29) expressed in terms of k and a/k^2 is separable and its general solution readily determined. In terms of a and k this solution is

$$\frac{a}{k} = \frac{Q}{\sqrt{\pi}}\left\{1 + \left(\frac{p}{2} - q\right)\frac{a}{k^2}\right\}^{(p-q)/(p-2q)}, \tag{30}$$

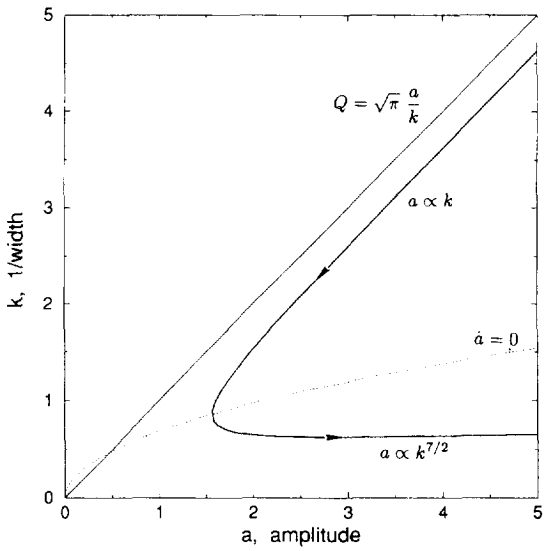

Fig. 3. An example of a trajectory in the (a, k) phase plane in the limit $k \to \infty$. The trajectory was computed from the relation (30), and arrows indicate the direction of increasing time t. As $k \to \infty$, the trajectories approach one of the two asymptotes, $a \propto k$ or, for $a/k^2 \gg 1$, $a \propto k^{7/2}$. Q denotes the total charge delivered by the pulse.

where $Q/\sqrt{\pi}$ is an arbitrary constant. As will be shown below, dividing by $\sqrt{\pi}$ gives Q the physical meaning of the charge delivered by the pulse. The graph of this relation in the (a, k) phase plane for fixed Q is depicted in Fig. 3 with the orientation determined by increasing time t. The two $k \to \infty$ asymptotes are $a \propto k$, which corresponds to the linear heat equation limit, and $a \propto k^{7/2}$, which corresponds to a local blowup of v. The rest of this section will discuss the physical meaning and the significance of the $a \propto k$ asymptote.

Consider the limit of a narrow pulse with $k \to \infty$ and $k^2 \gg a$. Then system (28) reduces further to

$$\dot{a} \sim -2k^2 a, \qquad \dot{k} \sim -2k^3. \tag{31}$$

From (31), solutions for $a(t)$ and $k(t)$ can be obtained as

$$a(t) \sim \frac{a_0}{\sqrt{t}}, \qquad k(t) \sim \frac{1}{2\sqrt{t}}, \tag{32}$$

where a_0 is an arbitrary constant. Inserting these $a(t)$ and $k(t)$ into (5) gives

$$v(x, t) = \frac{a_0}{\sqrt{t}} e^{-x^2/4t}, \tag{33}$$

which is the fundamental solution of the linear heat equation,

$$v_t = v_{xx}. \tag{34}$$

Now consider a corresponding limit applied to the reduced NLHE (25). Let $1/k_0$, $k_0 \gg 1$, be the largest scale in x. The scale of time that leads to the balance of v_t and v_{xx} is $1/k_0^2$. The magnitude of v is denoted by a_0, with the condition $a_0 \ll k_0^2$. In this case, v_t and v_{xx} are both of magnitude $k_0^2 a_0$, and $v(1-v)$ has magnitude a_0^2 which is much less than $k_0^2 a_0$. Under these conditions, the NLHE (25) asymptotically reduces to the linear heat equation (34). Therefore, the Gaussian pulse assumed in (5) as a parametric representation of v is a bona fide asymptotic solution of the NLHE in the limit $k_0 \to \infty$, $a_0 \ll k_0^2$.

The Gaussian pulse solutions of the linear heat equation (34) conserve total charge,

$$Q = \int_{-\infty}^{\infty} v \, dx = \sqrt{\pi}\,\frac{a}{k}. \tag{35}$$

Returning to the phase plane (a, k) of Fig. 2, note that as $k \to \infty$, the upper separatrix asymptotes to one of the lines of constant charge $Q = \sqrt{\pi}\,a/k$. Hence, in a limit of a very narrow initial pulse, the criterion for the initiation of propagation reduces to the condition that all threshold pulses deliver the same total charge Q.

4. Assessment of the results obtained with the projected dynamics

The use of the projected dynamics (26) to investigate the initiation of propagation results in a phase portrait (Fig. 2(a)) that confirms all the essential features predicted by McKean and Moll [12]: The division of the plane into sub- and super-critical data that are separated by a threshold curve and a motion of the phase point along this curve to a saddle point corresponding to the solution of the time-independent equation (6).

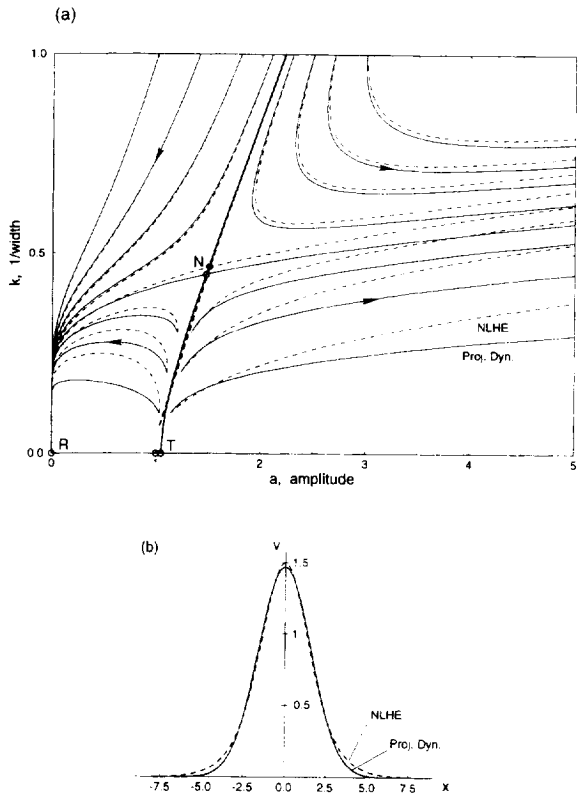

Fig. 4. The comparison of the phase portraits of the projected dynamics and the NLHE. (a) Solid trajectories are determined from ODEs (26) and dashed trajectories from the reduced NLHE (25). This phase plane contains two approximations of the critical nucleus solution: the lower circle corresponds to the saddle point (36) of the projected dynamics and the upper circle corresponds to the exact critical nucleus (37). In both cases, the width is measured as the e-folding distance; so k of the exact critical nucleus solution is 0.461 rather than 0.5. (b) The comparison of the two critical nucleus solutions shown in the phase plane of Panel (a).

In addition, the projected dynamics, while nonrigorous, produces a robust and a quantitatively good approximation to the true dynamics of the system. This agreement is demonstrated in Fig. 4(a), which compares the trajectories of the projected dynamics (solid lines) with the trajectories computed by a numerical solution of the NLHE (dashed lines).

The differences between these two sets of trajectories are the largest in the lower and the right parts of the phase plane, i.e., where the actual solution of the NLHE (25) is too broad or too tall to be well approximated by the Gaussian pulse (5). This is clearly seen when examining the $a \propto k^{7/2}$ asymptote of Fig. 3, corresponding to a local blowup of v. The relation $a \propto k^{7/2}$, determined based on the projected dynamics, suggests that the blowup is described by a similarity solution. This is true, but the exponent 7/2 is spurious. The large discrepancy between the projected dynamics and the NLHE trajectories indicate that the shape of the pulse near blowup is not Gaussian. The correct relation between amplitude a and width k near blowup, obtained from the reduced NLHE (25), is $a \propto k^2$ [18], not $a \propto k^{7/2}$.

Fig. 4(a) shows that the projected dynamics reproduces quite faithfully the position of the threshold separatrix and the critical nucleus solution. Under the projected dynamics, the critical nucleus has a Gaussian approximation

$$v_{\mathrm{cr}}(x) \approx 1.47\mathrm{e}^{-(0.447x)^2}. \tag{36}$$

As shown in Fig. 4(b), this approximation compares favorably to the exact critical nucleus solution (11), which after scaling (24) takes the form

$$v_{\mathrm{cr}}(x) = \tfrac{3}{2}\,\mathrm{sech}^2(\tfrac{1}{2}x). \tag{37}$$

The largest deviation between (36) and (37) is only 3.1% of the pulse amplitude.

As expected from the analysis presented in the previous section, the projected dynamics is most accurate for narrow pulses. Since the Gaussian pulse (5) is an asymptotic solution to the NLHE as $a, k \to \infty$, the asymptote $a \propto k$ of Fig. 3 gives a correct linear relation between the amplitude and the width of the pulse. If the pulse shape chosen in (5) were other than Gaussian, the description of pulse dynamics by the ODEs (26) for $a(t)$ and $k(t)$ would be degraded in the heat equation limit, but not badly. For instance, $v = a\,\mathrm{sech}^2(kx)$ might have been chosen since the critical nucleus solution (37) takes this form with $a = \frac{3}{2}$ and $k = \frac{1}{2}$. Constructing the ODEs for a and k based on the sech^2 profile, one finds that in the heat equation limit

$$\frac{a}{k^\gamma} \sim \text{constant}, \quad \text{where } \gamma = \tfrac{1}{15}\pi^2 + \tfrac{1}{4} \approx 0.908. \tag{38}$$

The actual Gaussian pulse solutions of the linear heat equation (34) conserve total charge Q (35), so the exponent γ should be 1. A similar problem was encountered for the other asymptote of Fig. 3, for which the projected dynamics gave an asymptotic relation $a \propto k^{7/2}$ rather than the correct $a \propto k^2$.

The fact that all initial data that lie on the $a, k \to \infty$ limit of the threshold curve carry the same total charge has been first recognized by Moll and Rosencrans [14] and Moll [15]. Using rectangular pulses as initial data, the threshold curve was found numerically and plotted as a log of the pulse amplitude versus log of its width [15, Fig. 8]. For the amplitudes in the range 0.5–1, the threshold curve is well approximated by a line of slope -1. The value of threshold μ in [15] is 0.2 and the threshold charge Q_{th} estimated from the graph is approximately 0.84. Moll also noted that as the initial pulse evolves in time and approaches the critical nucleus solution, its charge increases. In particular, in [15] the charge of $v_{\text{cr}}(x)$ is approximately 2.4, more than twice the charge of the threshold rectangular pulses of large amplitude.

The phenomenon of the constant total charge of the threshold pulses and its smallness relative to the charge of the critical nucleus can be easily explained using the projected dynamics. As discussed in the previous section, in the limit $a, k \to \infty$, the upper separatrix asymptotes to a line of constant charge (35). With the ratio $a/k \approx 1.4$, the threshold charge $Q_{\text{th}} \approx 1.4\sqrt{\pi}$. This estimate is scaled according to (24). The non-scaled charge is a function of the threshold μ,

$$Q_{\text{th}} = \sqrt{\pi\mu}\,\frac{a}{k} = 1.4\,\sqrt{\pi\mu}. \tag{39}$$

For $\mu = 0.2$, $Q_{\text{th}} \approx 1.1$, a value that is larger but comparable to 0.84 estimated from Fig. 8 of [15]. The discrepancy is due to different initial conditions (Gaussian versus rectangular pulses) and to the reduced, quadratic $f'(v)$ used by the projected dynamics. For $\mu = 0.2$, the Gaussian approximation of the critical nucleus (36) has total charge of 2.47, larger than the threshold charge and very close to the 2.4 estimate based on Moll's results [15].

Aronson and Weinberger in their 1975 paper [13] provided a method of estimating rigorous upper and lower bounds of the sub- and super-critical region. The rest of this section will compute these estimates for the special case of Gaussian initial data and compare them to the true threshold curve obtained from the numerical solution of the NLHE.

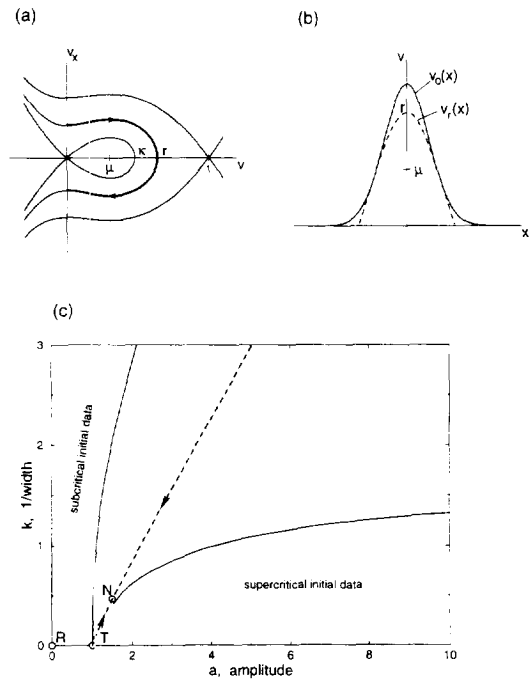

Fig. 5. (a) The phase portrait of the time independent equation (6) in the (v, v_x) plane. (b) The illustration of the sufficient condition for the supercritical pulse: The initial pulse $v_0(x)$ must fit over $v_r(x)$, the solution of Eq. (6) that corresponds to the trajectory shown in a heavy line in Panel (a). (c) The (a, k) phase plane showing in solid lines the boundaries of the sub- and super-critical regions computed numerically according to the Aronson and Weinberger estimates [13]. The dashed line shows the true position of the threshold curve (same as the dashed separatrices of Fig. 4(a)).

The sufficient condition for supercritical initial data given in [13] is based on comparison with solutions of the time-independent NLHE (6). Its first integral (7) gives the phase portrait shown in Fig. 5(a). If $(\kappa, 0)$ is the turning point of the homoclinic orbit, then choosing a turning point $(r, 0)$, $\kappa < r < 1$, defines a unique trajectory of the (v, v_x) plane (heavy line in Fig. 5(a)). The solution of (6) corresponding to this trajectory, $v_r(x)$, has a global maximum r at $x = 0$. The dashed line in Fig. 5(b) shows a portion of this solution with $v_r(x) > 0$. Given the sequence of $v_r(x)$, $\kappa < r < 1$,

the Aronson and Weinberger criterion can be stated as follows: The initial data $v_0(x)$ is supercritical if there is r, $\kappa < r < 1$, for which the positive portion of $v_r(x)$ lies underneath $v_0(x)$. This situation is depicted in Fig. 5(b) and the numerically determined approximation of the supercritical region is shown in Fig. 5(c).

The sufficient condition for subcritical initial data can be expressed as follows. Given $f'(v)$ as in (2), define

$$S(\rho) \equiv \max_{\mu<v<1} \frac{-f'(v)}{v-\rho} \quad \text{in } 0 < \rho < \mu. \tag{40}$$

An initial distribution $v_0(x)$ is subcritical if for some ρ, $0 < \rho < \mu$,

$$\int_{\alpha}^{\beta} (v_0(x) - \rho)\,\mathrm{d}x < \sqrt{\frac{2\pi}{\mathrm{e}S(\rho)}}\,(\mu - \rho), \tag{41}$$

where $\alpha < x < \beta$ is the interval where $v_0(x) > \rho$. Substituting for $v_0(x)$ a Gaussian pulse, (41) defines a region in the (a, k) plane corresponding to subcritical initial data. A numerically determined boundary of this region appears in Fig. 5(c).

The comparison of the sub- and super-critical regions computed according to Aronson and Weinberger [13] with the threshold curve determined by the numerical solution of the NLHE (solid line on the phase plane of Fig. 5(c)) shows that these estimates are very conservative, especially in the limit of tall and narrow pulses, $a, k \to \infty$. For the subthreshold condition (41), this limit can be examined directly and without the restriction to Gaussian initial data. Specifically, take

$$v_0(x) = \frac{1}{\varepsilon} V\left(\frac{x}{\varepsilon}\right), \tag{42}$$

where $V(x)$ is a positive integrable function and ε is a small positive number. In the limit $\varepsilon \to 0$, the left-hand side of (41),

$$\int_{\alpha}^{\beta} (v_0(x) - \rho)\,\mathrm{d}x \to \int_{-\infty}^{\infty} V(x)\,\mathrm{d}x, \tag{43}$$

becomes independent of ρ and, according to (35), represents the total charge Q delivered by the pulse. The right-hand side of (41) achieves its maximum at $\rho = 0$, with $S(0) = 1/4\,(1-\mu)^2$. Hence, the $\varepsilon \to 0$ limit of (41) is

$$Q < \sqrt{\frac{8\pi}{\mathrm{e}}}\,\frac{\mu}{(1-\mu)} \tag{44}$$

and states that a tall and narrow pulse is subcritical if its charge is sufficiently small.

The notion of the constant threshold charge, implied by (44), agrees with the results obtained in our study and in [14,15]. However, according to (44), in the limit $\mu \to 0$, Q_{th} is proportional to μ. The correct relationship (39), which was obtained using the projected dynamics, states that Q_{th} is proportional to $\sqrt{\mu}$. This is the reason why in Fig. 5(c), the boundary of the subcritical region departs from the actual threshold curve as the initial pulses become narrow. The increasing gap between the threshold curve and the boundary of the supercritical region can be similarly analyzed. In the $a \to \infty$ limit, the boundary of the supercritical region is given by $a/k^2 \to$ constant. This constant depends on μ, but converges to a positive value as $\mu \to 0$, causing the departure of the estimate from the actual threshold curve.

5. The role of the inactivation variable

The results presented in the three previous sections were obtained under the simplifying assumption that the inactivation variable y remained at its rest state and that the transmembrane potential v satisfied the reduced NLHE (25). This section re-introduces y into the model and examines its role in initiating propagation. In the limit of a small threshold $\mu \to 0$, the natural unit of y that is consistent with the units of v, x, t in (24) is μ^2. Making replacements (24) and $y \to \mu^2 y$, the FN model (1) takes the form

$$v_t = v_{xx} - v\,(1-v) - y, \qquad y_t = \frac{\varepsilon\alpha}{\mu}\,v - \varepsilon y. \tag{45}$$

In the limit $\mu \to 0$, $\varepsilon \to 0$ with ε/μ fixed, (45) reduces to

$$v_t = v_{xx} - v(1-v) - y, \qquad y_t = \varepsilon' v, \tag{46}$$

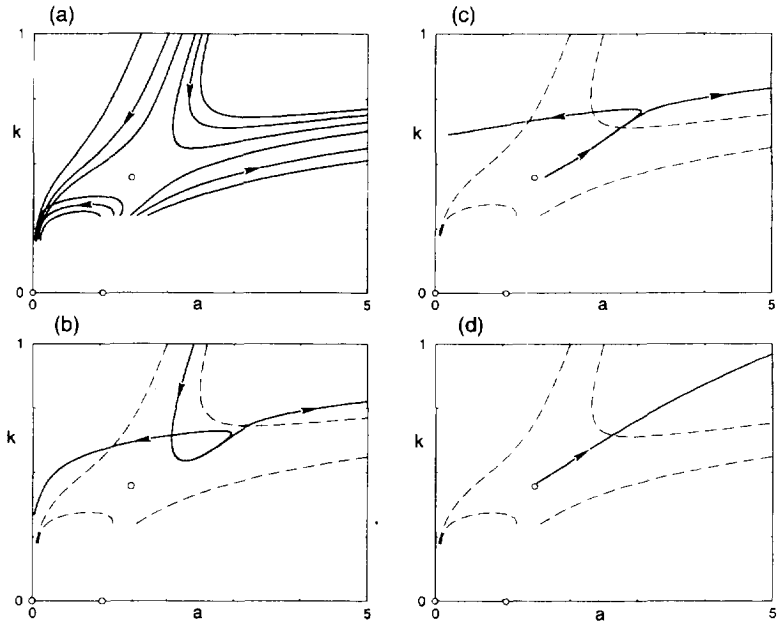

Fig. 6. The phase plane (a, k) of the reduced FN model (46). Panel (a) shows trajectories that originate away from the separatrices. Panel (b) shows two trajectories that originate very close to the upper separatrix and initially approach the critical nucleus. Panel (c) shows two trajectories that originate very close to the critical nucleus solution. In (b) and (c), the difference in the amplitude of the initial pulse between the trajectory that decays and the trajectory that blows up is 10^{-6}. Panel (d) shows the slow phase of the trajectories computed from Eqs. (49). In all panels, circles indicate positions of the rest state, the membrane threshold, and the critical nucleus solution (as in Fig. 2). Dashed lines show the representative four trajectories taken from Panel (a). The lower part of the graphs is left blank because, for small k, pulses become sufficiently broad to interfere with the ends of the fiber.

where $\varepsilon' \equiv \varepsilon\alpha/\mu = 0.21$, which can be considered small. This reduced FN model was solved numerically with the initial conditions

$$v(x, 0) = a(0)e^{-(k(0)x)^2}, \qquad y(0) = 0. \tag{47}$$

The amplitude and the width of the evolving pulse were measured at each time step and used to construct the trajectories on the (a, k) plane (Fig. 6).

Fig. 6(a) demonstrates that the general features of the (a, k) phase plane are the same, with or without the inactivation variable. As before, there are four types of trajectories, and most of them are not significantly affected by the presence of the inactivation variable. For initial conditions away from the ingoing separatrices of the phase plane in Fig. 2(a), $v(x, t)$ either decays to zero or blows up so rapidly that y undergoes little change from zero during the entire process. Hence, these evolutions are well described by the projected dynamics (26): Trajectories obtained from the numerical solution of the FN model (Fig. 6(a)) are indeed similar to trajectories of the projected dynamics phase plane (Fig. 2(a)).

The situation is drastically different for initial conditions near the ingoing separatrices of the phase plane in Fig. 2(a). Fig. 6(b) shows trajectories of the solutions in the (a, k) plane for two of these initial conditions. There is a rapid initial approach to the critical nucleus solution. Next, the phase point slowly drifts away, tracing out a curve that does not correspond to any trajectory in the phase plane of Fig. 2(a). This slow phase is unstable: After a duration of time which is extremely sensitive to the initial conditions, there is either a rapid decay of amplitude to zero or a blowup. Fig. 6(c) shows two trajectories that start very near the critical nucleus solution. Again, the phase point slowly drifts away from the critical nucleus and, depending on the small difference in the initial conditions, $v(x, t)$ eventually decays or blows up.

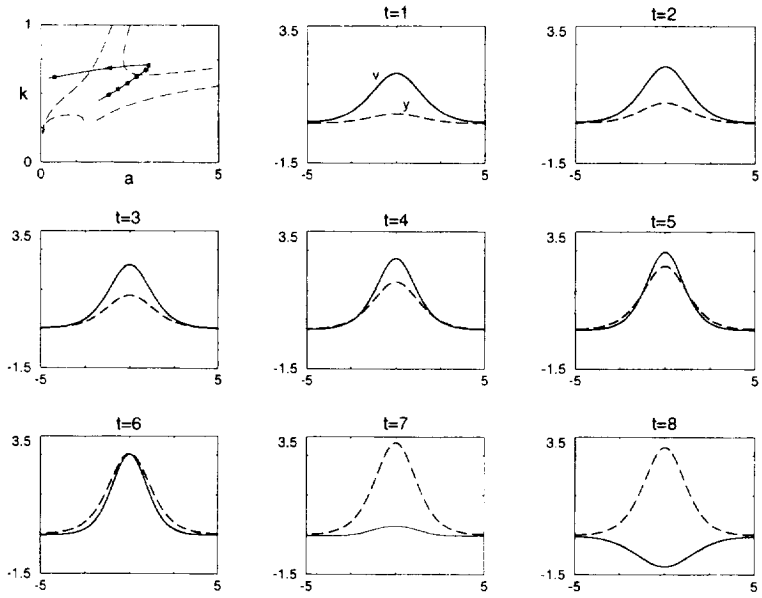

Fig. 7. The panel in the upper left corner shows the phase plane (a, k) of the FN model (46) with four trajectories that originate away from the separatrices and one trajectory that originates at the critical nucleus solution. On this trajectory, dots mark the instants of time $t = 1, 2, 3, \ldots, 7$. The remaining panels show spatial distribution of potential v (solid) and inactivation variable y (dashed) at times $t = 1, 2, 3, \ldots, 7$ and 8.

Fig. 7 shows a time sequence of configurations $v(x, t)$, $y(x, t)$ starting from initial conditions very near the critical nucleus solution. The time frames $t = 1, \ldots, 6$ correspond to the slow phase in which y undergoes a slow but cumulative growth according to the second equation of (46), and v simultaneously adjusts to the slowly changing y. The latter consists of a moderate growth in a and k. The time frames $t = 7, 8$ of Fig. 7 show a rapid collapse of $v(x, t)$ from a positive amplitude to a smaller negative amplitude. If the simulations were continued further in time, v and y would be observed to return to zero with the slow time constant $1/\varepsilon'$. As shown in Fig. 6(c), a slight increase in the initial condition would have led to a blowup instead of a collapse.

The brief inspection of Fig. 6 reveals that tracking the slow phase by direct numerical solutions of the reduced FN system (46) is difficult because the slow phase is highly unstable. A reduction of (46) under the limit $\varepsilon/\mu \to 0$ eliminates the rapidly growing deviations and allows to compute a simple approximation to the entire trajectory of the slow phase in the (a, k) plane. From (46), the time scale associated with the growth of y is $1/\varepsilon'$. Adopting $1/\varepsilon'$ as the unit of time, (46) transforms into

$$\varepsilon' v_t = v_{xx} - v(1 - v) - y, \qquad y_t = v. \tag{48}$$

In the limit $\varepsilon' \to 0$, Eqs. (46) reduce further to a system

$$v_{xx} - v(1 - v) = y, \qquad y_t = v. \tag{49}$$

which governs the slow phase. Fig. 6(d) depicts the numerical solution of the reduced system (49) starting from initial conditions equal to the critical nucleus solution (37). The resulting trajectory in the (a, k) phase plane approximately coincides with the slow portion of the trajectory in Fig. 6(c).

6. Discussion

The criterion for initiating propagation that emerges from this paper is that threshold pulses define a curve in the amplitude, width plane. Once the pulse width is

chosen, this curve determines the minimum amplitude of the pulse necessary to start propagation. Thus, the infinitely broad pulses (e.g., the space-clamped fiber) require an amplitude equal to the membrane excitation threshold μ. As the width of the pulse decreases, the requirement on the amplitude grows. In a limit of very narrow pulses, the pulse width and the amplitude are related by a linear relationship corresponding to a requirement that a constant amount of charge be delivered by the pulse.

This study found no indication of the existence of a liminal length, i.e., the minimum length of a fiber that the stimulus must raise above the threshold in order to initiate the propagation. On the contrary, the ingoing separatrices of the (a, k) phase plane bisect all pulse widths, and this indicates that, in theory, one should be able to start propagation with an arbitrarily narrow pulse as long as it carries a threshold charge. Thus, the liminal length does not appear to be an intrinsic property of the mechanism by which an external stimulus initiates propagation.

In the paper by Noble [11] the liminal length is defined as the width of the critical nucleus solution that is above the membrane excitation threshold μ. Note that the trajectories that originate close to the separatrices initially approach the critical nucleus (Fig. 2). For trajectories below the unstable manifold, pulses start broad and become narrower before they either decay to zero or blow up to infinity. For trajectories above the unstable manifold, the pulses start very narrow and broaden before they either decay or blow up. This may explain the existence of experimental data that agree with the liminal length hypothesis [9,10]. However, if the initial conditions are away from the separatrices, then the pulses, both broad and narrow, can develop into a propagating wavefront without approaching the critical nucleus solution. Hence, the agreement of experimental data with the liminal length hypothesis may be an artifact of the way by which the external stimulus was applied.

The results obtained in this paper required making several simplifying assumptions. The excitable medium was approximated by a one-dimensional fiber with an idealized dynamics based on the FN model. The external stimulation was represented by initial conditions on potential, thus assuming that the electrode charges the fiber instantaneously. In contrast, pulses used in clinical and experimental pacing have typical durations 0.1–2 ms [19], and representing them by initial conditions neglects the processes occurring during the pulse. Furthermore, the distribution of potential was assumed to have a Gaussian shape which is a close, but not an exact, representation of the potential established by point electrodes. Gaussian shaped pulses are also not a good representation for large electrodes that have edge effects associated with them [20]. Hence, the trajectories in the part of the phase plane corresponding to small k may depart from reality. However, limitations resulting from assuming Gaussian initial data will cause only a quantitative disagreement with the real process. As demonstrated by McKean and Moll [12], the qualitative features, such as the existence of the threshold separatrices, should hold true for any initial distribution of the transmembrane potential, as long as the pulse carries a finite charge. Finally, the FN dynamics was simplified by approximating the cubic nonlinearity by quadratic and thus neglecting the existence of the stable excited state. In consequence, the trajectories in the right part of the phase plane indicate that the amplitude increases without bounds instead of settling down to a steady state corresponding to the plateau of an action potential.

Despite these simplifications, the essential features of the initiation of propagation obtained with the simplified model remain true for more realistic models. As demonstrated in Section 4, the introduction of the inactivation variable y and solving the FN model numerically gives a phase plane (Fig. 6) which, with the exception of trajectories extremely close to the separatrices, does not differ appreciably from the phase plane of the projected dynamics (Fig. 2). Moreover, the same general features are also seen in the physiologically based models of the membrane. Fig. 8 shows the (a, k) phase plane obtained with the Luo–Rudy (LR) model of cardiac membrane [21]. One can clearly distinguish the same four types of trajectories. Also, the initial conditions that decay to zero and the initial conditions that lead to a propagating wavefront occupy nonoverlapping parts of the (a, k) phase plane. Thus, they indicate the existence of separatrices akin

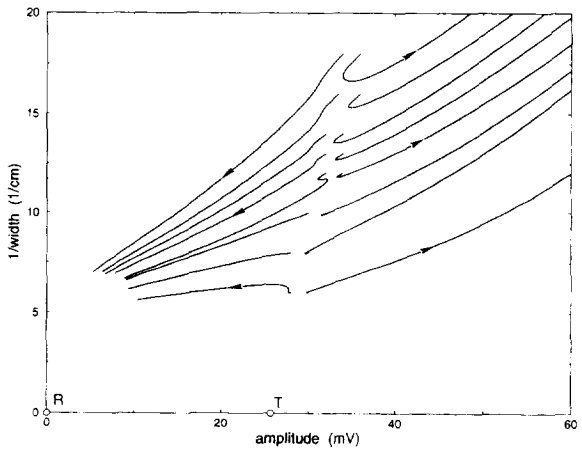

Fig. 8. Initiation of propagation in a physiologically based model of the membrane. The trajectories were obtained using the Luo–Rudy model of cardiac membrane and drawn on the (a, k) phase plane. The amplitude is measured with respect to the rest potential, −84 mV. Therefore, the origin $R(0, 0)$ corresponds to the rest state of the fiber. The trajectories turn either to the left (decay) or to the right (propagation), indicating the existence of separatrices that act as a threshold for propagation. Point $T(25.8, 0)$ denotes the threshold for the space-clamped Luo–Rudy membrane.

to those obtained with the projected dynamics. This qualitative agreement gives a reason to believe that the simplified analysis presented in this paper captures the essence of the mechanism by which local stimuli initiate propagating wavefronts.

Appendix A. Numerical simulations

In this paper, the values of the parameters, $\mu = 0.13$, $\varepsilon = 0.0094$, and $\alpha = 0.37$, were chosen to make system (1) equivalent to the equations in the original FitzHugh paper [1] (with FitzHugh's parameter $c = 5$ to enable propagation).

The phase plane of Fig. 2, corresponding to the projected dynamics (26) was constructed in the following way. ODEs (26) for a and k were solved using the forward Euler's method [22] with the time step $\mathrm{d}t = 0.01$. The trajectories were followed until a, k, or time reached a predetermined value.

The phase planes of Figs. 4 and 6 and the spatial distributions of v and y of Fig. 7 were constructed based on a one-dimensional fiber model of length $L = 10$ with the sealed-end boundary conditions. The evolution of v was computed from the reduced NLHE (23) with initial conditions (5). The evolution of v and y was computed from the reduced FN model (46) with initial conditions (47). A PDE for v was solved using the method of Crank–Nicolson [22], and the ODE for y was solved using the forward Euler's method. A time step $\mathrm{d}t = 0.01$ was used, and the fiber was discretized with $\mathrm{d}x = 0.01$.

To determine the boundary of the supercritical region shown in Fig. 5(c), a sequence of time-independent solutions to the NLHE $v_r(x)$ was determined from the following initial value problem:

$$v_{xx} - f'(v) = 0, \qquad v_x(0) = 0, \qquad v(0) = r. \tag{A.1}$$

The solutions of (A.1) were computed numerically using the NDSolve function of Mathematica [23]. Once a sequence of $v_r(x)$, $0.2 < r < 0.95$, was available, values of a and k were chosen and a Gaussian pulse (5) was generated and compared with all $v_r(x)$. The value of a was kept constant and k was interactively adjusted, until a narrowest pulse was found that exceeded at least one of the $v_r(x)$ functions (Fig. 5(b)).

The boundary of the subcritical region were computed from estimate (41). Assuming the limit $\mu \to 0$, function $S(\rho)$ was simplified to

$$S(\rho) \sim \tfrac{1}{4}(1 - \mu + \rho)^2. \tag{A.2}$$

Using (A.2) and a Gaussian pulse (5) as $v_0(x)$, (41) takes the form

$$\int_{-x_0(\rho)}^{x_0(\rho)} (a\mathrm{e}^{-(kx)^2} - \rho)\,\mathrm{d}x < \sqrt{\frac{8\pi}{\mathrm{e}}}\,\frac{\mu - \rho}{1 - \mu + \rho}, \tag{A.3}$$

where $x_0(\rho) = \sqrt{\ln(a/\rho)}/k$ and $0 \le \rho \le \mu$. For interactively chosen values of a and k, (A.3) was evaluated using Mathematica [23].

The slow phase of the trajectories, shown in Fig. 6(d), was computed using the same one-dimensional fiber model. The evolution of v and y was computed from Eqs. (49) with initial conditions equal to the critical nucleus solution (37). The boundary value problem for v was solved at each time step

using the iterative method of Newton–Raphson [24]. The ODE for y was solved using the forward Euler's method. The discretization steps were $dt = 0.05$ and $dx = 0.05$.

The phase plane of Fig. 8, corresponding to the LR model, was constructed based on the one-dimensional fiber model of length 1 cm and of radius 10 μm. Membrane capacitance C_m was 1 μF/cm^2, and internal resistance R_i was 0.47 kΩ cm [25]. Sealed-end boundary conditions were imposed at the ends. Initial conditions assigned to the gating variables corresponded to their rest states. The initial condition on v was the rest state potential of −84 mV plus a Gaussian pulse (5). A PDE for v was solved using the method of Crank–Nicolson, and ODEs for the gating variables were solved using the forward Euler's method. The time step was $dt = 0.01$ ms, and the fiber model was discretized with $dx = 0.00025$ cm.

Solutions of the NLHE and of the FN and LR models are not truly Gaussian. In order to draw the trajectories on the (a,k) phase plane, at each instant of time the amplitude a was taken as the maximum height of the pulse and the width $1/k$ was taken as the e-folding distance.

References

[1] R. FitzHugh, Impulses and physiological states in theoretical models of nerve membrane, Biophys. J. 1 (1961) 445–466.

[2] J. Nagumo, S. Arimoto and S. Yoshizawa, An active pulse transmission line simulating nerve axon, Proc. IRE 50 (1962) 2061–2070.

[3] H.P. McKean, Jr., Nagumo's equation, Adv. in Math. 4 (1970) 209–223.

[4] J. Rinzel and J.B. Keller, Traveling wave solutions of a nerve conduction equation, Biophys. J. 13 (1973) 1313–1337.

[5] R.G. Casten, H. Cohen and P.A. Lagerstrom, Perturbation analysis of an approximation to the Hodgkin–Huxley theory, Quart. Appl. Math. 32 (1975) 365–402.

[6] C.K.R.T. Jones, Stability of the travelling wave solution of the FitzHugh–Nagumo system, Trans. ASME 286 (1984) 431–469.

[7] J.J. Tyson and J.P. Keener, Singular perturbation theory of traveling waves in excitable media, (A review), Physica D 32 (1988) 327–361.

[8] W.A.H. Rushton, Initiation of the propagated disturbance, Proc. Roy. Soc. 124 (1937) 210–243.

[9] H.A. Fozzard and M. Schoenberg, Strength-duration curves in cardiac Purkinje fibres: Effects of liminal length and charge distribution, J. Physiol. 226 (1972) 593–618.

[10] F.W. Lindemans and J.J.D. van der Gon, Current thresholds and liminal size in excitation of heart muscle, Cardiovasc. Res. 12 (1978) 477–485.

[11] D. Noble, The relation of Rushton's 'liminal length' for excitation to the resting and active conductances of excitable cells, J. Physiol. 266 (1972) 573–591.

[12] H.P. McKean and V. Moll, Stabilization to the standing wave in a simple caricature of the nerve equation, Comm. Pure Appl. Math. 39 (1986) 485–529.

[13] D.G. Aronson and H.F. Weinberger, Nonlinear diffusion in population genetics, combustion, and nerve propagation, in: Partial Differential Equations and Related Topics, ed. J.A. Goldstein, Lecture Notes Mathematics, Vol. 446 (Springer, Berlin, 1975) pp. 5–49.

[14] V. Moll and S.I. Rosencrans, Calculation of the threshold surface for nerve equations, SIAM J. Appl. Math. 50 (1990) 1419–1441.

[15] V. Moll, Polygonal approximation to the flow on the critical surface for the bistable equation, Comput. Math. Appl. 25 (1993) 45–51.

[16] D. Terman, Threshold phenomena for a reaction–diffusion system, J. Differential Equations 47 (1983) 406–443.

[17] P.C. Fife and J.B. McLeod, The approach of solutions of nonlinear diffusion equations to travelling front solutions, Arch. Rational Mech. Anal. 65 (1977) 335–361.

[18] Y. Giga and R. Kohn, Asymptotic self similar blowup of semilinear heat equations, Comm. Pure Appl. Math. 38 (1985) 297–319.

[19] R.E. Ideker, D.W. Frazier, W. Krassowska and J.M. Wharton, Physiologic effects of electrical stimulation in cardiac muscle, in: The Electrical Therapy of Cardiac Arrhythmias, eds. S. Saksena and N. Goldschlager (Saunders, Philadelphia, PA, 1990) pp. 357–370.

[20] Y. Kim, J.B. Fahy and B.J. Tupper, Optimal electrode design for electrosurgery, defibrillation, and external cardiac pacing, IEEE Trans. Biomed. Eng. 33 (1986) 845–853.

[21] C-H. Luo and Y. Rudy, A model of the ventricular cardiac action potential: Depolarization, repolarization, and their interaction, Circ. Res. 68 (1991) 1501–1526.

[22] C.F. Gerald, Applied Numerical Analysis, 2nd Ed. (Addison-Wesley, Readings, MA, 1978).

[23] S. Wolfram, Mathematica. A System of Doing Mathematics by Computer, 2nd Ed. (Addison–Wesley, Redwood City, CA, 1991).

[24] G. Dahlquist and A. Björck, Numerical Methods (Prentice-Hall, Englewood Cliffs, NJ, 1974).

[25] S. Weidmann, Electrical constants of trabecular muscle from mammalian heart, J. Physiol. 210 (1970) 1041–1054.